Journal of Power and Energy Engineering, 2026, 14(2), 1-18
https://www.scirp.org/journal/jpee
ISSN Online: 2327-5901
ISSN Print: 2327-588X

Optimal Operation Strategy of Distributed Integrated Energy Microgrid Considering Ladder-Type Carbon Trading

Li Jiang, Dong Han*

School of Mechanical Engineering, University of Shanghai for Science and Technology, Shanghai, China
Email: *han_dong@usst.edu.cn

How to cite this paper: Jiang, L. and Han, D. (2026) Optimal Operation Strategy of Distributed Integrated Energy Microgrid Considering Ladder-Type Carbon Trading. *Journal of Power and Energy Engineering*, **14**, 1-18.
https://doi.org/10.4236/jpee.2026.142001

Received: January 17, 2026
Accepted: February 3, 2026
Published: February 6, 2026

Copyright © 2026 by author(s) and Scientific Research Publishing Inc.
This work is licensed under the Creative Commons Attribution-NonCommercial International License (CC BY-NC 4.0).
http://creativecommons.org/licenses/by-nc/4.0/

Open Access

Abstract

Distributed Integrated Energy Microgrid, as a key infrastructure for the low-carbon transition of regional energy systems, faces critical challenges in achieving optimal operation—primarily due to limited energy endowments and insufficient internalization of carbon costs. To address these issues, this paper proposes an optimal operation method for distributed integrated energy microgrids considering ladder-type carbon trading. Firstly, a reward-punishment incentive-based ladder-type carbon trading mechanism is introduced to control the carbon emission level of microgrids through differentiated carbon prices. Secondly, a low-carbon economic operation objective targeting the minimum comprehensive operation cost of the microgrid itself is constructed, and the original problem is transformed into a mixed-integer linear programming problem, which is solved using the CPLEX solver. Finally, case studies using data from the Shanghai Caojing Integrated Energy Center demonstrate that the proposed method achieves excellent economic efficiency and low-carbon performance, thereby confirming its feasibility and engineering applicability.

Keywords

Distributed Integrated Energy Microgrid, Ladder-Type Carbon Trading, Low-Carbon Economy, Multi-Energy Coupling

1. Introduction

With the continuous increase in the penetration rate of renewable energy in power systems, the operation of energy systems is facing multiple challenges, such as enhanced resource diversity, inherent temporal volatility of renewable energy out-

puts, and growing demand for load flexibility. Microgrids, leveraging their characteristics of distributed deployment and autonomous regulation, have been widely applied in balancing regional energy supply and demand as well as local regulation. However, traditional microgrids with a single energy structure are constrained by limited energy endowments, insufficient operational economy, and underutilized synergistic potential, making it difficult to meet the operational requirements of complex multi-energy systems. To address this, constructing a Distributed Integrated Energy Microgrid (DIEM) that integrates various types of energy conversion and carbon resource response capabilities to achieve the synergistic coupling, flexible conversion, and cascaded utilization of multiple energy forms has become a key pathway to improve the resilience and economy of energy systems [1].

In recent years, the optimal operation of microgrids has attracted extensive attention in academic circles and industrial practices [2]. Reference [3] established a microgrid model including distributed wind and photovoltaic power generation systems, combined heat and power systems, electric boilers, fuel cells, and energy storage systems, laying a foundation for multi-energy synergistic operation. Reference [4] developed a day-ahead centralized optimal scheduling model for a multi-microgrid system with combined cooling, heating, and power involving electrical energy interaction, aiming to minimize the total operational cost of the multi-microgrid system. In addition to improving the economy and flexibility of system operation, reducing the system's carbon emission level is also one of the important objectives of energy management. Carbon trading mechanisms have been gradually introduced into the low-carbon economic optimization management of energy systems; for example, Reference [5] explored operational optimization strategies under carbon constraints for microgrids containing micro gas turbines, and Reference [6] studied the electricity-carbon trading model for community microgrids. However, most of the aforementioned studies embed carbon-related factors into the optimization model in the form of static carbon prices or penalty terms, and have not yet systematically constructed a comprehensive characterization of quota allocation, dynamic pricing, and incentive feedback in carbon trading mechanisms [7]-[9]. This to a certain extent limits the dynamic guiding role of carbon cost signals in operational strategies. Notably, for microgrids with inherent characteristics of time-varying emissions, cost sensitivity, and heterogeneous scales, the ladder-type carbon trading mechanism exhibits obvious theoretical superiority over a static carbon tax. Firstly, it matches the time-varying emission characteristics of microgrids: microgrids integrate volatile renewable energy and multi-energy conversion equipment, leading to significant temporal fluctuations in carbon emission intensity, and the ladder-type mechanism's differentiated pricing based on emission intervals can realize targeted emission reduction regulation in high-emission periods, which is difficult for a static carbon tax with a uniform rate. Secondly, it balances the dual goals of economy and low-carbon: as small-scale energy systems, microgrids are sensitive to operational costs,

and the static carbon tax's one-way punishment increases financial burdens, while the ladder-type mechanism's "reward-punishment" logic effectively reduces the net cost of emission reduction. Thirdly, it adapts to heterogeneous operational scales: microgrids vary in size and load types, and the adjustable parameters of the ladder-type mechanism enable customized regulation, while the static carbon tax's "one-size-fits-all" rate lacks targeted regulation effects. Therefore, constructing a low-carbon optimal operation model for microgrids and introducing a scientific price incentive mechanism to achieve the synergistic optimization of economy and low-carbon performance is of great theoretical value and practical significance.

To this end, targeting the low-carbon operation needs of DIEM, this paper proposes an optimal operation model considering a reward-punishment incentive-based ladder-type carbon trading mechanism, with the core goal of realizing explicit quantitative accounting of carbon costs and synergistic optimal scheduling of multi-energy flows. Meanwhile, a comprehensive operational cost system for microgrids covering the entire process is constructed, specifically including external interaction costs, unit operation and maintenance costs, wind and solar curtailment costs, operation and maintenance costs of energy storage systems, and carbon trading costs. Taking the minimization of this comprehensive operational cost as the core objective, this study provides a feasible optimization scheme for the low-carbon economic operation of DIEMs, making up for the deficiencies of existing research in the refined characterization of carbon trading mechanisms and the synergistic management of multiple costs.

2. Architecture Design and Multi-Energy Equipment Modeling of Distributed Integrated Energy Microgrid

2.1. Architecture Design of DIEM

The interior of DIEM is composed of three layers: the energy supply side, conversion and coupling side, and demand side [10], forming a system architecture oriented toward multi-energy complementarity as shown in **Figure 1**. Compared with traditional microgrids, DIEM has three technical advantages: improving the local consumption capacity of renewable energy through electricity-heat-hydrogen multi-energy coupling; integrating Carbon Capture, Utilization and Storage (CCUS) and Power-to-Gas (P2G) technologies to form a closed-loop carbon cycle path; and possessing flexible trading capabilities to participate in both the electricity market and carbon trading market, realizing the joint optimization of economic and low-carbon objectives. Through the coordinated operation of internal multi-energy coupling equipment, DIEM constructs an integrated operation system of "production-conversion-storage-trading"; externally, by interfacing with the carbon trading market, it achieves multi-energy complementarity and explicit quantitative accounting of carbon costs, providing a physical carrier and market mechanism support for the low-carbon operation of microgrids under the new power system.

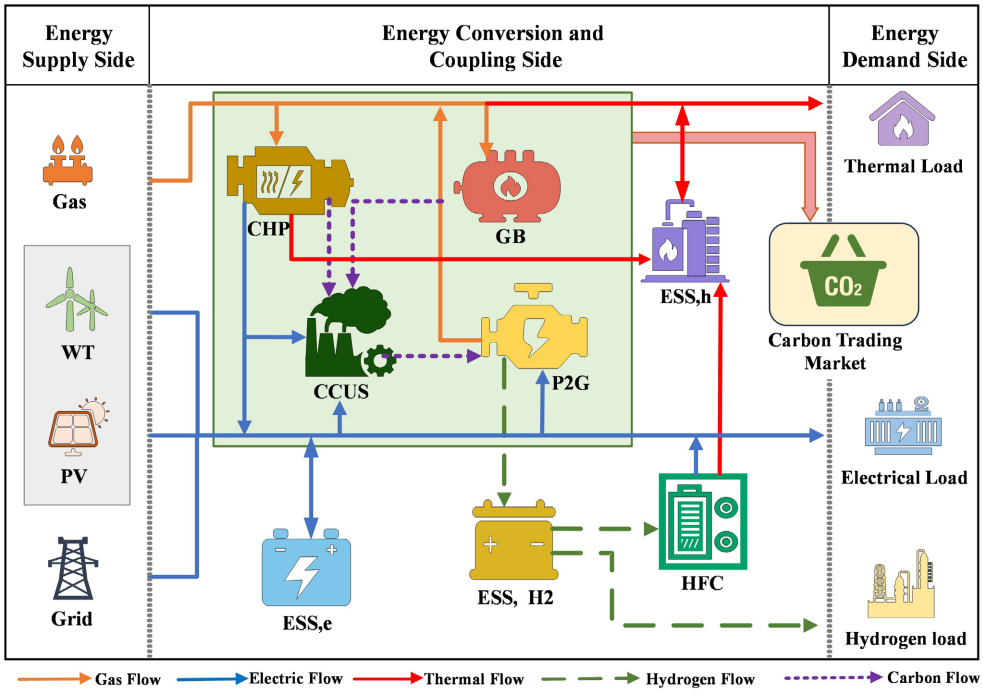

Figure 1. Architecture design of DIEM.

2.2. Mathematical Modeling of Energy Coupling for Multi-Energy Conversion Equipment

Based on the equipment operation and energy conversion mechanisms, mathematical descriptions are established for the core equipment in DIEM, including Combined Heat and Power (CHP), Gas Boiler (GB), Power to Gas (P2G), Hydrogen Fuel Cell (HFC), Carbon Capture, Utilization, and Storage (CCUS), and Energy Storage System (ESS) By constructing energy input-output mapping functions, the conversion efficiency characteristics, operational boundary constraints, and multi-energy flow coupling relationships are comprehensively considered, providing a physical layer constraint foundation for the optimal operation of microgrids.

2.2.1. CHP

CHP unit is a device that produces both electricity and thermal energy. It uses fuels such as natural gas for combustion to generate thermal energy, which is then converted into electricity. Meanwhile, the waste heat generated during the power generation process is utilized for heating, cooling, or industrial production processes.

$$P_t^{CHP} = N_t^{CHP} \eta_E^{CHP} LHV_{CH_4} \tag{1}$$

$$P_t^{CHP} \geq \max\left\{P_{\min}^{CHP} - k_{\min} H_t^{CHP}, k_l\left(H_t^{CHP} - H_0^{CHP}\right)\right\} \tag{2}$$

$$P_t^{CHP} \leq P_{\max}^{CHP} - k_{\max} H_t^{CHP} \tag{3}$$

$$H_t^{CHP} \geq 0 \tag{4}$$

$$H_t^{CHP} = \frac{P_t^{CHP} P_h \left(1 - \eta_E^{CHP} - \eta_{loss}^{CHP}\right)}{\eta_E^{CHP}} \tag{5}$$

P_t^{CHP}, H_t^{CHP} —Power generation power and heat generation power of CHP.

H_0^{CHP} —Heat power corresponding to the minimum power generation power of CHP.

$k_{\min}$, $k_{\max}$ —Electrical-thermal conversion coefficients of CHP unit corresponding to the minimum and maximum output power.

k_l —Linear supply slope of electrical and thermal power of CHP.

η_E^{CHP}, η_{loss}^{CHP} —Power generation efficiency and loss coefficient of CHP.

P_h —Cogeneration factor.

N_t^{CHP} —Natural gas consumption of CHP.

LHV_{CH_4} —Low heating value of natural gas, *i.e.*, the heat released when unit mass of CH_4 is completely burned.

$P_{\min}^{CHP}$, $P_{\max}^{CHP}$ —Upper and lower limits of power generation power of CHP.

2.2.2. GB

GB is a heating equipment that uses gaseous fuels such as natural gas or liquefied petroleum gas. Compared with traditional coal-fired boilers, it generally has higher combustion efficiency, enabling more sufficient release of thermal energy, and at the same time, the exhaust gas generated during its combustion contains fewer pollutants.

$$H_t^{GB} = N_t^{GB} \eta^{GB} LHV_{CH_4} \tag{6}$$

$$H_{min}^{GB} \le H_t^{GB} \le H_{max}^{GB} \tag{7}$$

H_t^{GB} —Heat generation power of GB.

N_t^{GB} —Natural gas consumption of GB.

η^{GB} —Heat generation efficiency of GB.

H_{min}^{GB}, H_{max}^{GB} —Upper and lower limits of heat generation power of GB.

2.2.3. P2G

P2G equipment can realize two types of energy conversion: it converts electrical energy into hydrogen in an electrolyzer (EL); part of the hydrogen is used for hydrogen energy supply, and the other part reacts with CO_2 in a methane reactor (MR) to produce methane.

$$P_{t,\mathrm{H_2}}^{\mathrm{EL}} = \eta^{\mathrm{EL}} P_t^{\mathrm{EL}} \tag{8}$$

$$P_{t,\mathrm{H_2}}^{\mathrm{EL}} = P_{t,\mathrm{H_2}}^{\mathrm{P2G}} + P_{t,\mathrm{H_2}}^{\mathrm{MR}} \tag{9}$$

$$N_{t,\mathrm{CH_4}}^{\mathrm{MR}} = \frac{\eta^{\mathrm{MR}} P_{t,\mathrm{H_2}}^{\mathrm{MR}}}{LHV_{CH_4}} \tag{10}$$

$$\begin{cases} P_{\min}^{EL} \le P_{t,\mathrm{H_2}}^{\mathrm{EL}} \le P_{\max}^{EL} \\ \Delta P_{\min}^{EL} \le P_{t+1,\mathrm{H_2}}^{\mathrm{EL}} - P_{t,\mathrm{H_2}}^{\mathrm{EL}} \le \Delta P_{\max}^{EL} \\ P_{\mathrm{H_2},\min}^{MR} \le P_{t,\mathrm{H_2}}^{MR} \le P_{\mathrm{H_2},\max}^{MR} \\ \Delta P_{\mathrm{H_2},\min}^{MR} \le P_{t+1,\mathrm{H_2}}^{MR} - P_{t,\mathrm{H_2}}^{MR} \le \Delta \mathrm{P}_{\mathrm{H_2},\max}^{MR} \end{cases} \tag{11}$$

$P_{t,\mathrm{H}_2}^{\mathrm{EL}}$ —Hydrogen production power of EL.

η^{EL} —Operating efficiency of EL.

P_t^{EL} —Electrical energy input power of EL.

$P_{t,\mathrm{H}_2}^{\mathrm{P2G}}$ —Hydrogen production power of P2G equipment used for hydrogen energy supply.

$P_{t,\mathrm{H}_2}^{\mathrm{MR}}$ —Hydrogen input power of MR.

$N_{t,\mathrm{CH}_4}^{\mathrm{MR}}$ —Methane production volume of MR.

η^{MR} —Operating efficiency of MR.

$P_{\min}^{EL}$, $P_{\max}^{EL}$ —Upper and lower limits of electrical energy input power of EL.

$P_{H_2,\min}^{MR}$, $P_{H_2,\max}^{MR}$ —Upper and lower limits of hydrogen input power of MR.

$\Delta P_{\min}^{EL}$, $\Delta P_{\max}^{EL}$ —Upper and lower limits of ramp rate of EL.

$\Delta P_{H_2,\min}^{MR}$, $\Delta P_{H_2,\max}^{MR}$ —Upper and lower limits of ramp rate of MR.

2.2.4. HFC

Hydrogen energy can be converted into electrical energy and thermal energy through HFC equipment.

$$P_{t,\mathrm{e}}^{\mathrm{HFC}} = \eta_{\mathrm{e}}^{\mathrm{HFC}} P_{t,\mathrm{H}_2}^{\mathrm{HFC}} \tag{12}$$

$$H_{t,\mathrm{h}}^{\mathrm{HFC}} = \eta_{\mathrm{h}}^{\mathrm{HFC}} P_{t,\mathrm{H}_2}^{\mathrm{HFC}} \tag{13}$$

$$\begin{cases} 0 \le P_{t,\mathrm{H}_2}^{\mathrm{HFC}} \le P_{\mathrm{H}_2,\max}^{\mathrm{HFC}} \\ k_{\min}^{\mathrm{HFC}} \le \dfrac{P_{t,\mathrm{e}}^{\mathrm{HFC}}}{H_{t,\mathrm{h}}^{\mathrm{HFC}}} \le k_{\max}^{\mathrm{HFC}} \\ \Delta P_{\mathrm{H}_2,\min}^{\mathrm{HFC}} \le P_{t+1,\mathrm{H}_2}^{\mathrm{HFC}} - P_{t,\mathrm{H}_2}^{\mathrm{HFC}} \le \Delta P_{\mathrm{H}_2,\max}^{\mathrm{HFC}} \end{cases} \tag{14}$$

$P_{t,\mathrm{e}}^{\mathrm{HFC}}$ —Electrical energy power generated by HFC.

$\eta_{\mathrm{e}}^{\mathrm{HFC}}$ —Electrical conversion efficiency of HFC.

$P_{t,\mathrm{H}_2}^{\mathrm{HFC}}$ —Hydrogen power consumed by HFC.

$H_{t,\mathrm{h}}^{\mathrm{HFC}}$ —Thermal energy power generated by HFC.

$\eta_{\mathrm{h}}^{\mathrm{HFC}}$ —Thermal conversion efficiency of HFC.

$P_{\mathrm{H}_2,\max}^{\mathrm{HFC}}$ —Maximum hydrogen power consumed by HFC.

$k_{\min}^{\mathrm{HFC}}$, $k_{\max}^{\mathrm{HFC}}$ —Upper and lower limits of the electrical-thermal ratio of HFC.

2.2.5. CCUS

A post-combustion capture system is adopted to capture CO_2 generated from the combustion of natural gas in CHP systems and GB. Part of the captured CO_2 is transported to the P2G system for methane production, and the other part is sequestered to reduce carbon emissions. Uncaptured CO_2 is emitted into the atmosphere.

$$\begin{cases} E_t^{CHP} = \mu^{CHP} P_t^{CHP} \\ E_t^{GB} = \mu^{GB} H_t^{GB} \\ E_t = E_t^{CHP} + E_t^{GB} \\ E_t^{out} = \left(1 - \eta_c^{CCUS}\right) E_t \\ E_{t,c}^{CCUS} = \eta_c^{CCUS} E_t \end{cases} \tag{15}$$

$$\begin{cases} E_{t,c}^{CCUS} = E_{t,CO_2}^{P2G} + E_{t,s}^{CCUS} \\ E_{t,CO_2}^{P2G} = \lambda_{CO_2}^{MR} P_{t,H_2}^{MR} \end{cases} \tag{16}$$

$$\begin{cases} P_t^{CCUS} = P_{t,c}^{CCUS} + P_{t,s}^{CCUS} = \lambda_c^{CCUS} E_{t,c}^{CCUS} + \lambda_s^{CCUS} E_{t,s}^{CCUS} \\ P_{t,\min}^{CCUS} \le P_t^{CCUS} \le P_{t,\max}^{CCUS} \\ \Delta P_{\min}^{CCUS} \le P_{t+1}^{CCUS} - P_t^{CCUS} \le \Delta P_{\max}^{CCUS} \end{cases} \tag{17}$$

E_t^{CHP}, E_t^{GB} —Carbon emissions generated by CHP and GB.

μ^{CHP}, μ^{GB} —Carbon emission factors of CHP and GB.

E_t —Carbon emissions generated by DIEM.

E_t^{out} —Carbon emissions released into the atmosphere without capture.

η_c^{CCUS} —Carbon capture efficiency of CCUS technology.

$E_{t,c}^{CCUS}$ —Carbon emissions captured by CCUS.

E_{t,CO_2}^{P2G} —CO_2 captured by CCUS used for methane production.

$E_{t,s}^{CCUS}$ —CO_2 captured by CCUS used for storage.

$\lambda_{CO_2}^{MR}$ —Carbon consumption coefficient of MR for methane production.

P_t^{CCUS} —Total energy consumption of CCUS.

λ_c^{CCUS}, λ_s^{CCUS} —Power consumption coefficients for unit carbon capture and storage.

$P_{t,\min}^{CCUS}$, $P_{t,\max}^{CCUS}$ —Upper and lower limits of CCUS power.

$\Delta P_{\min}^{CCUS}$, $\Delta P_{\max}^{CCUS}$ —Upper and lower limits of CCUS ramp rate.

2.2.6. ESS

Three types of energy storage devices are considered, namely batteries, heat storage tanks, and hydrogen storage tanks, and the State of Charge (SOC) variable is introduced to describe the state of each system.

1) When the system is in the charging state:

$$SOC_{\mathrm{ESS},t}^{\mathrm{e/h/H_2}} = SOC_{\mathrm{ESS},t-1}^{\mathrm{e/h/H_2}} + P_{\mathrm{ESS},t,\mathrm{chr}}^{\mathrm{e/h/H_2}} \cdot \eta_{\mathrm{ESS},chr}^{\mathrm{e/h/H_2}} \Big/ C_{\mathrm{ESS}}^{\mathrm{e/h/H_2}} \tag{18}$$

2) When the system is in the discharging state:

$$SOC_{\mathrm{ESS},t}^{\mathrm{e/h/H_2}} = SOC_{\mathrm{ESS},t-1}^{\mathrm{e/h/H_2}} - P_{\mathrm{ESS},t,dis}^{\mathrm{e/h/H_2}} \Big/ \left(\eta_{\mathrm{ESS},dis}^{\mathrm{e/h/H_2}} \cdot C_{\mathrm{ESS}}^{\mathrm{e/h/H_2}} \right) \tag{19}$$

$SOC_{\mathrm{ESS},t}^{\mathrm{e/h/H_2}}$ —SOC of the electricity/heat/hydrogen storage systems.

$P_{\mathrm{ESS},t,\mathrm{chr}}^{\mathrm{e/h/H_2}}$, $P_{\mathrm{ESS},t,dis}^{\mathrm{e/h/H_2}}$ —Charging/discharging power of electricity/heat/hydrogen.

$\eta_{\mathrm{ESS},chr}^{\mathrm{e/h/H_2}}$, $\eta_{\mathrm{ESS},dis}^{\mathrm{e/h/H_2}}$ —Charging/discharging efficiency of the electricity/heat/hydrogen storage systems.

$C_{\mathrm{ESS}}^{\mathrm{e/h/H_2}}$ —Capacity of the electricity/heat/hydrogen storage systems.

$$\begin{cases} SOC_{\mathrm{ESS},\min}^{\mathrm{e/h/H_2}} \le SOC_{\mathrm{ESS},t}^{\mathrm{e/h/H_2}} \le SOC_{\mathrm{ESS},\max}^{\mathrm{e/h/H_2}} \\ k_{\mathrm{ESS},chr}^{\mathrm{e/h/H_2}} P_{\mathrm{ESS},chr,\min}^{\mathrm{e/h/H_2}} \le P_{\mathrm{ESS},t,chr}^{\mathrm{e/h/H_2}} \le k_{\mathrm{ESS},chr}^{\mathrm{e/h/H_2}} P_{\mathrm{ESS},chr,\max}^{\mathrm{e/h/H_2}} \\ k_{\mathrm{ESS},dis}^{\mathrm{e/h/H_2}} P_{\mathrm{ESS},dis,min}^{\mathrm{e/h/H_2}} \le P_{\mathrm{ESS},t,dis}^{\mathrm{e/h/H_2}} \le k_{\mathrm{ESS},dis}^{\mathrm{e/h/H_2}} P_{\mathrm{ESS},dis,\max}^{\mathrm{e/h/H_2}} \end{cases} \tag{20}$$

$$\begin{cases} k_{\mathrm{ESS},chr}^{\mathrm{e/h/H_2}} + k_{\mathrm{ESS},dis}^{\mathrm{e/h/H_2}} \le 1 \\ k_{\mathrm{ESS},chr}^{\mathrm{e/h/H_2}}, k_{\mathrm{ESS},dis}^{\mathrm{e/h/H_2}} \in \{0,1\} \end{cases} \tag{21}$$

$$\begin{cases} \Delta P^{e/h/H_2}_{ESS,chr,\min} \le P^{e/h/H_2}_{ESS,t,chr} - P^{e/h/H_2}_{ESS,t-1,chr} \le \Delta P^{e/h/H_2}_{ESS,chr,\max} \\ \Delta P^{e/h/H_2}_{ESS,dis,\min} \le P^{e/h/H_2}_{ESS,t,dis} - P^{e/h/H_2}_{ESS,t-1,dis} \le \Delta P^{e/h/H_2}_{ESS,dis,\max} \end{cases} \quad (22)$$

$SOC^{e/h/H_2}_{ESS,\min}$, $SOC^{e/h/H_2}_{ESS,\max}$ —Upper and lower limits of the SOC.

$P^{e/h/H_2}_{ESS,chr,\min}$, $P^{e/h/H_2}_{ESS,chr,\max}$, $P^{e/h/H_2}_{ESS,dis,min}$, $P^{e/h/H_2}_{ESS,dis,\max}$ —Upper and lower limits of charging and discharging power.

$\Delta P^{e/h/H_2}_{ESS,chr,\min}$, $\Delta P^{e/h/H_2}_{ESS,chr,\max}$, $\Delta P^{e/h/H_2}_{ESS,dis,\min}$, $\Delta P^{e/h/H_2}_{ESS,dis,\max}$ —Upper and lower limits of the ramp rate of ESS.

Among them, $k^{e/h/H_2}_{ESS,chr}$ and $k^{e/h/H_2}_{ESS,dis}$ are flag coefficients for charging and discharging states, which are 0 - 1 variables. If the value is 1, it indicates charging; if the value is 0, it indicates discharging. Therefore, ESS cannot perform charging and discharging simultaneously

2.3. Modeling of Reward-Punishment Incentive-Based Ladder-Type Carbon Trading Mechanism

At present, China's carbon trading market is in a stage of accelerated construction and improvement, with remarkable results achieved in pilot projects in many regions. Based on the consumption-side accounting principle, the mechanism for DIEM to participate in the carbon trading market is modeled, following the basic principle of "who emits, who bears". The carbon emission responsibility boundary is defined as follows: 1) As a terminal energy producer and consumer, DIEM assumes full responsibility for operational carbon emissions; 2) Indirect carbon emissions caused by DIEM's external power purchase shall be uniformly calculated in accordance with the regional power grid benchmark emission factor announced by the state; 3) ESS and HFC only involve energy conversion, do not directly consume fossil energy, and do not generate additional carbon emissions during operation, so they are not included in the carbon emission accounting boundary.

Under this mechanism, the regulatory authority provides DIEM with free initial carbon emission allowances. When DIEM's actual carbon emissions are lower than the allowances, the remaining allowances can be sold in the carbon trading market for profit; otherwise, it is required to purchase allowances for the excess emission part. This carbon trading mechanism mainly consists of three parts: initial allocation of carbon emission rights, actual carbon emissions, and ladder-type carbon trading costs [11] [12].

2.3.1. Initial Allocation Model of Carbon Emission Rights

Carbon allowances are allocated free of charge to incentivize DIEM to save energy and reduce emissions. According to the definition of carbon emission boundaries, the main sources of DIEM's carbon emissions include: 1) Indirect carbon emissions caused by DIEM purchasing electricity from the main grid (consumption-side accounting); 2) Direct carbon emissions generated by equipment such as CHP and GB consuming natural gas. Therefore, the initial carbon allowance model is as follows:

$$\begin{cases} E^0 = E^0_{e,buy} + E^0_{CHP} + E^0_{GB} \\ E^0_{e,buy} = \chi_e \sum_{t=1}^{T} p_t^{buy} \\ E^0_{CHP} = \chi_h \sum_{t=1}^{T} \left(P_t^{CHP} + H_t^{CHP} \right) \\ E^0_{GB} = \chi_h \sum_{t=1}^{T} H_t^{GB} \end{cases} \tag{23}$$

E^0 —Carbon quota for DIEM.

$E^0_{e,buy}$ —Carbon quota for DIEM's electricity purchase from the upper-level grid.

E^0_{CHP} —Carbon quota for CHP.

E^0_{GB} —Carbon quota for GB.

p_t^{buy} —Electricity purchase volume of DIEM from the upper-level grid.

χ_e —Carbon quota per unit power consumption of coal-fired units.

χ_h —Carbon quota per unit natural gas consumption of natural gas-fired units.

2.3.2. Actual Carbon Emission Model

Considering that the electricity purchased from the upper-level grid comes from coal-fired power units, and CCUS can capture CO_2 and generate methane in P2G, the actual carbon emission model based on the carbon emission responsibility boundary is as follows:

$$\begin{cases} E_f = E_{e,buy,f} + E^{CHP,GB}_{total,f} - E_{CCUS,f} \\ E_{e,buy,f} = \sum_{t=1}^{T} \left(a_1 + b_1 p_t^{buy} + c_1 \left(p_t^{buy} \right)^2 \right) \\ E^{CHP,GB}_{total,f} = \sum_{t=1}^{T} \left(a_2 + b_2 \left(P_t^{CHP} + H_t^{CHP} + H_t^{GB} \right) + c_2 \left(P_t^{CHP} + H_t^{CHP} + H_t^{GB} \right)^2 \right) \\ E_{CCUS,f} = \sum_{t=1}^{T} \varpi P_t^{CCUS} \end{cases} \tag{24}$$

E_f —Actual carbon emissions of DIEM.

$E_{e,buy,f}$ —Indirect carbon emissions from DIEM's electricity purchase from the upper-level grid.

$E^{CHP,GB}_{total,f}$ —Direct carbon emissions of CHP and GB.

$E_{CCUS,f}$ —CO_2 capture volume of CCUS.

ϖ —Capture parameter.

$a_1 / b_1 / c_1$, $a_2 / b_2 / c_2$ —Carbon emission calculation parameters for coal-fired units and natural gas-fired units.

2.3.3. Reward-Punishment Incentive-Based Ladder-Type Carbon Trading Model

To strengthen the incentive and constraint functions of the carbon market, a reward-punishment incentive-based ladder-type carbon trading mechanism is introduced. Based on a segmented increasing price strategy, an incentive mechanism characterized by "increasing costs for excess emissions and increasing returns for surplus allowances" is formed.

The carbon trading volume of DIEM is expressed as follows:

$$E_t = E_f - E^0 \tag{25}$$

The mathematical model of the ladder-type carbon trading for DIEM is as follows:

$$C_{CO_2} = \begin{cases} -\alpha_{CO_2}^{\text{base}}\left(1+\varepsilon\right)\left(E_t - l\right) - \alpha_{CO_2}^{\text{base}} l, -2l \le E_t \le -l \\ -\alpha_{CO_2}^{\text{base}} E_t, -l \le E_t \le 0 \\ \alpha_{CO_2}^{\text{base}} E_t, 0 \le E_t \le l \\ \alpha_{CO_2}^{\text{base}}\left(1+\nu\right)\left(E_t - l\right) + \alpha_{CO_2}^{\text{base}} l, l \le E_t \le 2l \\ \alpha_{CO_2}^{\text{base}}\left(1+2\nu\right)\left(E_t - 2l\right) + \alpha_{CO_2}^{\text{base}}\left(2+\nu\right) l, 2l \le E_t \le 3l \\ \alpha_{CO_2}^{\text{base}}\left(1+3\nu\right)\left(E_t - 3l\right) + \alpha_{CO_2}^{\text{base}}\left(3+3\nu\right) l, 3l \le E_t \le 4l \\ \alpha_{CO_2}^{\text{base}}\left(1+4\nu\right)\left(E_t - 4l\right) + \alpha_{CO_2}^{\text{base}}\left(4+6\nu\right) l, 4l \le E_t \le 5l \end{cases} \tag{26}$$

C_{CO_2} —Carbon trading cost.

l —Carbon emission interval length.

ε —Price compensation coefficient for surplus interval.

ν —Price growth coefficient for excess interval.

3. Optimal Operation Model of Distributed Integrated Energy Microgrid

3.1. Objective Function

The DIEM aims to minimize its own comprehensive operational cost, which includes external interaction costs, unit operation and maintenance costs, wind and solar curtailment costs, operation and maintenance costs of energy storage systems, and carbon trading costs (see Section 2.3.3 for details, which will not be repeated here).

$$\max F^{DIEM} = -\left(C_{utility} + C_{units} + C_{cut} + C_{ESS} + C_{CO_2}\right) \tag{27}$$

$$C_{utility} = \sum_{t=1}^{T}\left[\left(\lambda_t^{CH_4} N_t^{CH_4}\right) + \left(\lambda_t^{Mb} P_t^{\text{buy}} - \lambda_t^{Ms} P_t^{\text{sell}}\right)\right] \tag{28}$$

$$\begin{aligned} C_{units} = \sum_{t=1}^{T}\Big[& \alpha_1 P_t^{CHP} + \beta_1\left(P_t^{CHP}\right)^2 + \alpha_2 H_t^{GB} + \beta_2\left(H_t^{GB}\right)^2 \\ & + \alpha_3 P_t^{P2G} + \alpha_4 P_{t,H_2}^{HFC} + \alpha_5 P_t^{CCUS} + \alpha_6\Big] \end{aligned} \tag{29}$$

$$C_{cut} = \lambda_{cur}\left(P_{t,cur}^{WT} + P_{t,cur}^{PV}\right) \tag{30}$$

$$C_{ESS} = \sum_{t=1}^{T} \varsigma\left(P_{ESS,T,chr}^{e/h/H_2} + P_{ESS,T,dis}^{e/h/H_2}\right) \tag{31}$$

F^{DIEM} —Benefits of DIEM.

$C_{utility}$ —External interaction costs.

C_{units} —Unit operation and maintenance costs.

C_{cut} —Wind and solar curtailment costs.

C_{ESS} —Operation and maintenance costs of energy storage systems.
$\lambda_t^{CH_4}$ —Natural gas purchase price.
$\alpha_1 \sim \alpha_6$, $\beta_1 \sim \beta_2$ —Unit operation cost coefficients.
λ_{cur} —Wind and solar curtailment cost coefficient.
ς —Degradation cost per unit energy for charging and discharging.

3.2. Constraints

3.2.1. Energy Supply-Demand Balance Constraint

$$\begin{aligned} &P_t^{PV} + P_t^{WT} + P_t^{buy} + P_{t,\mathrm{e}}^{\mathrm{HFC}} + P_t^{CHP} + P_{\mathrm{ESS},t,dis}^{\mathrm{e}} \\ &-P_t^{\mathrm{EL}} - P_t^{CCUS} = P_t^{sell} + P_{\mathrm{ESS},t,chr}^{\mathrm{e}} + L_t^e \end{aligned} \tag{32}$$

$$H_t^{CHP} + H_t^{GB} + H_{t,\mathrm{h}}^{\mathrm{HFC}} + P_{\mathrm{ESS},t,dis}^{\mathrm{h}} = P_{\mathrm{ESS},t,chr}^{\mathrm{h}} + L_t^h \tag{33}$$

$$P_{t,\mathrm{H_2}}^{\mathrm{P2G}} + P_{\mathrm{ESS},t,dis}^{\mathrm{H_2}} = P_{t,\mathrm{H_2}}^{MR} + P_{t,\mathrm{H_2}}^{\mathrm{HFC}} + P_{\mathrm{ESS},t,chr}^{\mathrm{H_2}} + L_t^{H_2} \tag{34}$$

3.2.2. Exchange Power Constraint

$$N_{min}^{CH_4} \le \left| N_t^{CH_4} \right| \le N_{max}^{CH_4} \tag{35}$$

3.2.3. Natural Gas Flow Balance Constraint

$$N_t^{CH_4} + N_{t,\mathrm{CH_4}}^{\mathrm{MR}} = N_t^{CHP} + N_t^{GB} \tag{36}$$

3.2.4. Carbon Emission Flow Balance Constraint

$$E_t^{CHP} + E_t^{GB} - E_{t,c}^{CCUS} = E_t^{out} \tag{37}$$

$$E_t^{CHP} + E_t^{GB} - E_{t,CO_2}^{P2G} - E_{t,s}^{CCUS} = E_t^{out} \tag{38}$$

4. Case Study Analysis

4.1. Basic Settings

The basic data in this paper is derived from the actual operational data of the Shanghai Caojing Integrated Energy Center. Among them, the multi-energy load data and renewable energy output data are directly obtained from this center. The parameters of the carbon trading mechanism are set as shown in Table 1, and the multi-energy loads and forecast of renewable energy outputs are detailed in Figure 2.

Table 1. Parameters of the carbon trading mechanism.

Parameters	Value	Parameters	Value
χ_e	0.537	a_2	3
χ_h	0.367	b_2	0.85
ϖ	1.02	c_2	0.71
a_1	5	ε	0.2
b_1	0.25	ν	0.25
c_1	0.54	l	50

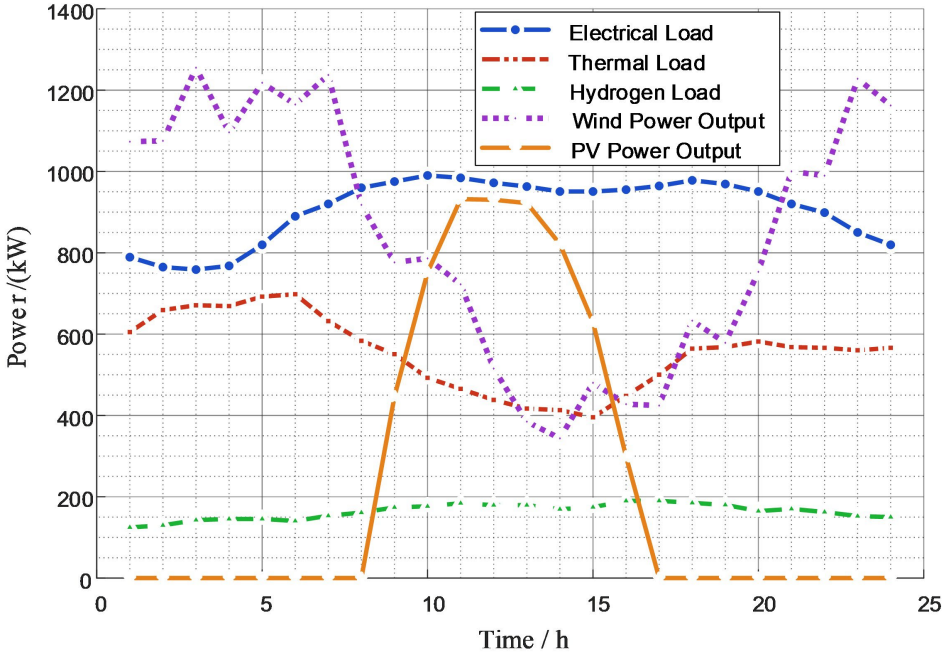

Figure 2. Multi-energy loads and forecast of renewable energy outputs.

4.2. Solution Settings and Computational Environment

The mixed-integer linear programming model established in this paper is solved by the CPLEX solver based on the MATLAB platform. The key solver parameters are set as follows: the duality gap tolerance is set to 1.00e−04, and the number of parallel computing threads is set to 28. All calculations are implemented on a standard desktop computer with the following hardware configuration: Intel (R) Core (TM) i7-14700HX processor, Windows 11 (64-bit) operating system, and MATLAB R2024b. The total computation time for the whole process to achieve optimal convergence is only 0.13 seconds.

4.3. Analysis of Optimal Operation Strategies

Figure 3 reveals the typical output characteristics of renewable energy in DIEM: PV output presents an obvious unimodal distribution, reaching the peak power during the midday period from 11:00 to 15:00; wind power output exhibits stronger randomness and intermittency. Such differentiated output characteristics lead to power surplus in the system during the midday period when PV generation is high; while there is a power supply gap during the evening peak load period from 19:00 to 22:00.

To further analyze the impact of the carbon trading mechanism on the multi-energy operation of DIEM, two comparative scenarios are set as follows:

Scenario 1: The carbon trading mechanism is not considered, with the sole objective of minimizing the economic operation cost;

Scenario 2: The ladder-type carbon trading mechanism is considered, *i.e.*, the carbon trading cost is included in the optimization model.

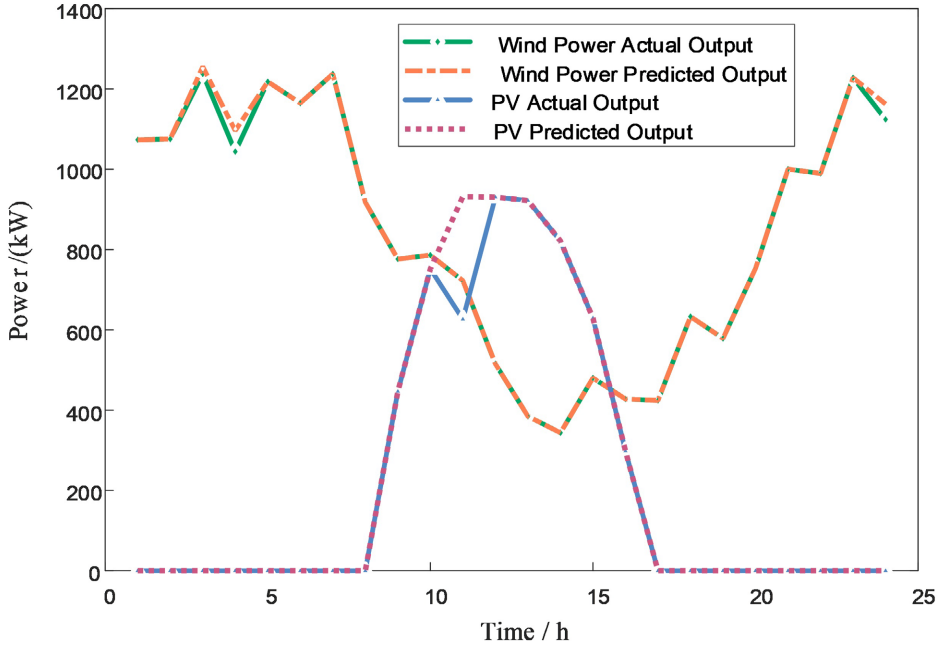

Figure 3. Renewable energy generation output.

With the results shown in **Figure 4**. At the power level, Scenario 1 features frequent and high-level unit output, leading to power surplus in multiple periods but high carbon emissions; by contrast, Scenario 2 reduces the proportion of high-carbon power generation, emphasizes environmental constraints, cuts down power-selling behavior significantly, and moves toward load self-balance. In thermal dispatch, Scenario 1 requires increased CHP cogeneration heat output to match its continuous operation, resulting in obvious thermal energy redundancy, while Scenario 2 shortens CHP operation time, compensates by raising GB heat output, and uses thermal energy storage to smooth heat load fluctuations, thus achieving flexible and economically matched thermal dispatch. In the hydrogen energy path, the P2G system is more effectively utilized in Scenario 2—during the midday peak of renewable energy output, electricity is allocated to P2G for hydrogen production, which improves local power consumption efficiency and enhances hydrogen reserve adjustability—whereas in Scenario 1, HFC is only used to convert hydrogen into electricity and heat during demand peaks.

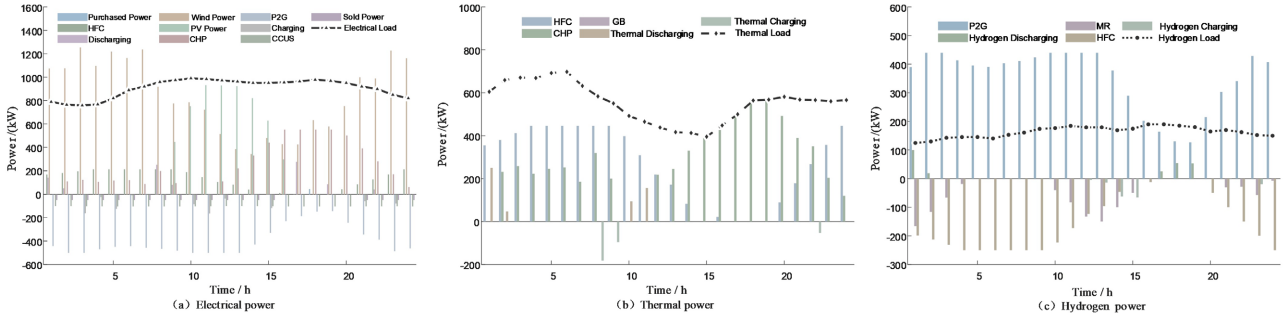

Figure.4 Scenario 1

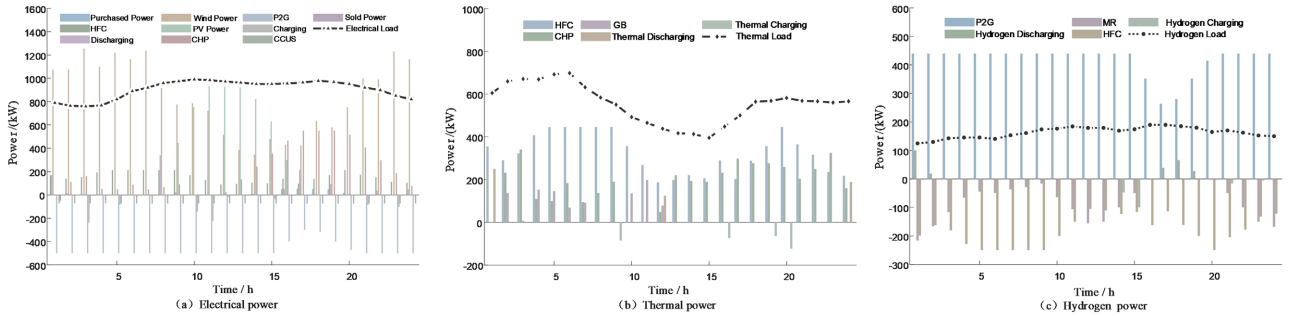

Figure.4 Scenario 2

Figure 4. Energy optimization operation results of DIEM under Scenario 1 and Scenario 2.

4.4. Economic and Environmental Benefit Analysis

Figure 5 illustrates the carbon emission distribution of DIEM under the two scenarios, and the results indicate that the carbon trading mechanism exerts a significant guiding effect on carbon emission behaviors. Since Scenario 1 does not consider carbon cost constraints, the system operation strategy is mainly oriented toward economic objectives, which leads to the priority activation of conventional high-carbon units such as CHP to meet load demands and thus results in relatively high carbon emissions. After the introduction of the conventional stepped carbon trading mechanism in Scenario 2, DIEM realizes the capture and storage of CO_2 during peak carbon emission periods by virtue of CCUS technologies, while reasonably controlling the output of high-carbon equipment. Consequently, the net carbon emissions decrease significantly, which demonstrates the regulatory flexibility and emission reduction guiding capability based on the stepped carbon trading mechanism.

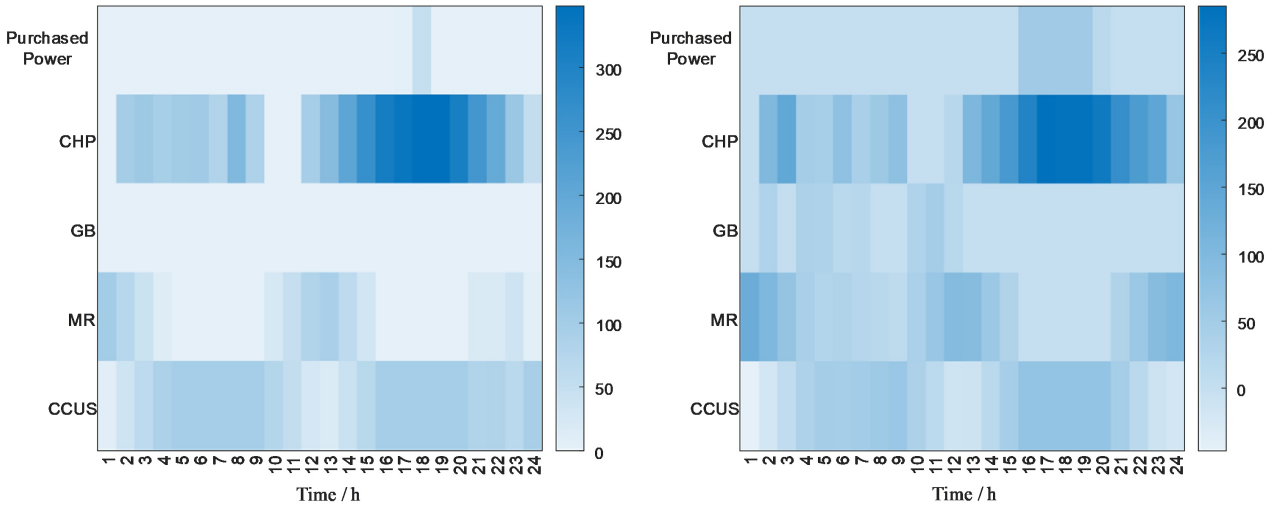

Figure.5 Scenario1

Figure.5 Scenario2

Figure 5. Carbon emissions distribution of the DIEM under Scenario 1 and Scenario 2.

To verify the synergistic effects of economic benefits and environmental per-

formance under different carbon emission strategies, a comparative analysis is conducted on the two typical scenarios. The results are presented in Table 2: Scenario 2 incurs a carbon trading cost of 408.11 CNY, with carbon emissions reduced from 3211.17 kg to 2467.56 kg. On the basis of achieving a 23.16% carbon emission reduction rate, the comprehensive operation cost increases by approximately 4.71%, which reflects the restrictive effect of explicit carbon cost on system operation strategies. The above results indicate that the proposed carbon trading mechanism possesses both carbon regulation flexibility and price guiding capability, providing effective support for DIEM to achieve the dual optimization goals under carbon constraint conditions.

Table 2. Comparison of benefits before and after implementing the ladder-type carbon trading mechanism.

Parameters	Scenario 1	Scenario 2
Carbon Emission/kg	3 211.17	2 467.56
Carbon Trading Cost/CNY	/	408.11
Comprehensive Operation Cost/CNY	15 421.07	16 148.12

4.5. Sensitivity Analysis of Key Parameters in Ladder-Type Carbon Trading Mechanism

As shown in Figure 6, to investigate the impact of policy stringency on the low-carbon economic operation of the DIEM, a sensitivity analysis is conducted on two key parameters of the ladder-type carbon trading mechanism: interval length l and price growth coefficient v.

For interval length l, when l is in the range of (0.5, 2], the interval length is relatively small, and the system purchases carbon emission rights quotas at ladder prices for most periods, resulting in high carbon trading costs and thus low carbon emissions. When l is in the range of (2, 5], the interval length is relatively large; due to the inherent load demand of the DIEM, with the increase of l, the volume of carbon emission rights quotas purchased at high-gradient prices decreases, leading to lower carbon trading costs. As the carbon emission cost gradually decreases, the system's carbon emissions increase accordingly. When l is in the range of (5, 8], carbon emissions are all traded at the benchmark price and the first gradient price, and the impact of l on carbon emissions is minor, so carbon emissions reach stability; with the further increase of l, the system's carbon trading cost decreases continuously, and the total operation cost also decreases gradually.

For price growth coefficient v, when v is in the range of [0, 0.4), with the increase of v, the carbon trading cost increases accordingly. To reduce the carbon trading cost, the system adjusts the output distribution of internal equipment to reduce carbon emissions, resulting in a gradual decrease in carbon emissions and a continuous increase in total operation cost. When v is in the range of [0.4, 0.8], the output of internal equipment has been adjusted to the optimal low-carbon operation state, and the impact of v on carbon emissions is relatively small, so

carbon emissions tend to be stable; with the further increase of *r*, the carbon trading cost and total operation cost continue to rise. Overall, interval length mainly regulates the tightness of carbon emission quotas, while price growth coefficient dominates the incentive intensity of carbon prices, and both parameters jointly determine the trade-off between carbon emissions and economic operation of the DIEM.

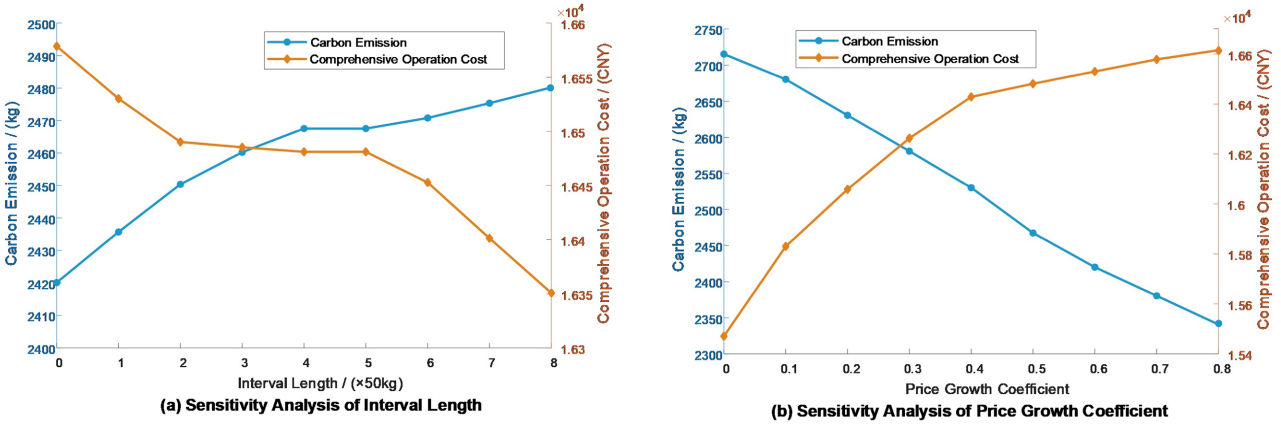

Figure 6. Sensitivity analysis of key parameters.

5. Conclusions

1) Constructing a DIEM that integrates multiple types of energy conversion technologies and carbon resource response capabilities enables the synergistic coupling, flexible conversion, and cascade utilization of various energy forms. This architecture breaks the isolation of traditional single-energy systems, achieves deep complementarity among electricity, heat, and hydrogen through multi-energy coupling equipment, and improves the comprehensive energy utilization efficiency by virtue of the cascade utilization of energy with different grades.

2) The stepped carbon trading mechanism can effectively balance the carbon trading cost and the comprehensive system operation cost while ensuring the emission reduction effect. Compared with the scenario without carbon trading participation, this mechanism reduces carbon emissions by 23.16%, while the comprehensive operation cost only increases by 4.71%, demonstrating superior environmental-economic synergistic benefits and regulatory adaptability.

3) Simulation examples verify the feasibility of the proposed method under the carbon market synergy mechanism. Specifically, during periods of high renewable energy output, the method not only promotes the local consumption of renewable energy and the feedback of surplus electricity to the grid, but also effectively improves the utilization rate of green energy.

Conflicts of Interest

The authors declare no conflicts of interest regarding the publication of this paper.

References

[1] Li, H., Zhu, J.Z. and Dong, H.J. (2025) Two-Stage Distributionally Robust Optimization Scheduling for Multi-Energy Microgrid Considering Covariate Factors. *Proceedings of the CSEE*, **45**, 822-834.

[2] Liu, Y.X., Yao, L.Z. and Zhao, B. (2024) Low-Carbon Economic Dispatch of Distribution Network-Microgrid Clusters Considering Flexible Clustering. *Automation of Electric Power Systems*, **48**, 59-68.

[3] Sun, P., Yun, T. and Chen, Z. (2021) Multi-Objective Robust Optimization of Multi-Energy Microgrid with Waste Treatment. *Renewable Energy*, **178**, 1198-1210. https://doi.org/10.1016/j.renene.2021.06.041

[4] Zhang, Y.M., Li, J.R. and Ji, X.Q. (2025) Bi-Level Game Dispatch of Park Integrated Energy System Considering Decision-Making Synergy of Electricity-Carbon Markets. *Automation of Electric Power Systems*, **49**, 45-59.

[5] Wei, L.S., Yang, B.B. and Sun, R.X. (2023) Optimal Scheduling of Microgrid Based on Improved BBO Algorithm. *Journal of System Simulation*, **35**, 1075-1085.

[6] Zhong, X., Zhong, W., Liu, Y., Yang, C. and Xie, S. (2022) Cooperative Operation of Battery Swapping Stations and Charging Stations with Electricity and Carbon Trading. *Energy*, **254**, Article 124208. https://doi.org/10.1016/j.energy.2022.124208

[7] Liu, L.Y., Jiang, K. and Liu, N. (2024) Multi-Agent Energy-Carbon Sharing Mechanism for Parks Based on Stackelberg Game. *Proceedings of the CSEE*, **44**, 2119-2131.

[8] Sun, Q., Wang, X., Liu, Z., Mirsaeidi, S., He, J. and Pei, W. (2022) Multi-Agent Energy Management Optimization for Integrated Energy Systems under the Energy and Carbon Co-Trading Market. *Applied Energy*, **324**, Article 119646. https://doi.org/10.1016/j.apenergy.2022.119646

[9] Liu, X. (2025) Strategy Research on Variable Load Carbon Price and Demand Response of Integrated Energy System Based on Stackelberg Game and Cooperative Game. *Energy*, **328**, Article 136579. https://doi.org/10.1016/j.energy.2025.136579

[10] Hou, H., Ge, X., Yan, Y., Lu, Y., Zhang, J. and Dong, Z.Y. (2024) An Integrated Energy System "Green-Carbon" Offset Mechanism and Optimization Method with Stackelberg Game. *Energy*, **294**, Article 130617. https://doi.org/10.1016/j.energy.2024.130617

[11] Lei, L. and Wu, N. (2024) An Optimal Scheduling Strategy for Electricity-Thermal Synergy and Complementarity among Multi-Microgrid Based on Cooperative Games. *Renewable Energy*, **237**, Article 121575. https://doi.org/10.1016/j.renene.2024.121575

[12] Zhao, C., Liu, Q., Han, D., Niu, P. and Wu, S. (2024) Decentralized Energy Trading Framework with Personalized Pricing for Energy Community Embedded with Shared Energy Storage. *Electric Power Systems Research*, **235**, Article 110562. https://doi.org/10.1016/j.epsr.2024.110562